UNIVERSITY OF CALIFORNIA

Santa Barbara

The Influence of the Montecito Debris Flows on Landcover in Carpinteria Salt Marsh

A Thesis submitted in partial satisfaction of the

requirements for the degree Master of Arts

in Geography

by

Germán David Silva

Committee in charge:

Professor Jennifer Y. King, Co-Chair

Professor Dar A. Roberts, Co-Chair

Professor Joseph P. McFadden

September 2021

The thesis of Germán David Silva is approved.

_____
Joseph P. McFadden

_____
Dar A. Roberts, Committee Co-Chair

_____
Jennifer Y. King, Committee Co-Chair

August 2021

The Influence of the Montecito Debris Flows on Landcover in Carpinteria Salt Marsh

by

Germán David Silva

ACKNOWLEDGEMENTS

No research or piece of writing is ever accomplished by one person alone, even during a global pandemic. Every writer has someone that they brainstorm ideas with, that provides input as they progress through their work, someone who edits, and people supporting them during writer's block, and I am no exception to this rule. I have many people to thank for helping me through the process of completing this Master Thesis. Firstly, I would like to thank my committee composed of Drs. Jennifer King, Dar Roberts, and Joe McFadden for all the guidance, feedback, and mentoring they provided me through the entire process of working on this research from the formulation of a research idea through the writing of this manuscript. I would also like to thank the Terrestrial Earth Surface Processes group for listening to my many presentations and providing useful feedback and ideas as I progressed through my research. Many of my classmates and lab mates helped me through the many milestones I accomplished during this project, but I want to especially thank Chelsie McWhorter, David Miller, and Michael Allen for the help, feedback, and guidance they provided me through the entire process. I want to thank Alex Feldwinn for all the tech support and times that he restarted my computer so that I could continue working from home during the pandemic. Lastly, I want to thank the National Science Foundation Graduate Research Fellowship Program for funding me as I pursued this research. I truly could not have done it without all of you.

Dedicated to my mother for encouraging me to always chase after my goals

ABSTRACT

The Influence of the Montecito Debris Flows on Landcover in Carpinteria Salt Marsh

by

Germán David Silva

The Montecito debris flows of 9 January 2018 deposited sediment along many portions of the Santa Barbara coast, including Carpinteria Salt Marsh Reserve. Since disturbances have the potential to impact the ecosystem services and functions that wetlands provide, an understanding of how the ecosystem at Carpinteria Salt Marsh Reserve responded to this disturbance is important to its ongoing management. However, a lack of opportunity to collect field data around the time of disturbance makes this task difficult to complete by field methods. To address this gap, Sentinel-2 imagery from four dates (November 2017, January 2018, November 2018, November 2020) was used to calculate landcover fractions, normalized difference vegetation index (NDVI), and modified anthocyanin reflectance index (mARI) and used in tandem with random forest classification to produce maps of landcover before, during, and after the debris flow. Post-classification change detection was then performed on the classified maps to track changes in landcover through time. Results from the random forest classification showed that NDVI and green vegetation fractions were the most important variables in classifying landcover, though this varied on a date-by-date basis; error matrices indicated that the model had high accuracy with values of 0.994, 0.920, 0.956. and 0.963 for the respective dates. Change detection

shows a pattern of returning to pre-debris flow vegetation extent in the marsh. While total vegetated area experienced little change (0.12% increase), there was a change in the extent of vegetation type with high marsh vegetation shifting to mid marsh vegetation in regions near where increases in bare soil landcover occurred. These results show that disturbance due to debris flow can cause vegetation changes which may affect ecosystem function, such as decrease primary productivity and marsh resilience to further disturbance, that will need to be taken into consideration when managing depositional event prone wetlands.

TABLE OF CONTENTS

LIST OF TABLES & FIGURES

I. Introduction

In December 2017, the Thomas Fire burned an area of 1140 km^2 in the Santa Ynez Mountains, making it the largest fire in California's history at the time (Andone 2018; Kean *et al*. 2019). The burned areas experienced an increased risk of debris flows from the catchments in the Santa Barbara, CA area; and, a month later, a heavy rain event mobilized soils from the burn area and triggered a depositional event known as the Montecito debris flows (Kean *et al.* 2019). The debris flows resulted in approximately 680,000 m^3 of sediment being deposited across urban and natural areas along the Santa Barbara Coast (Kean *et al*. 2019). Among the areas impacted was one University of California Natural Reserve System site, the Carpinteria Salt Marsh Reserve.

Coastal salt marshes, like Carpinteria Salt Marsh, are dynamic ecosystems found at the interface between marine and terrestrial environments. These productive ecosystems play important roles in coastal resilience via a variety of ecosystem services, such as accreting sediments, sequestering carbon, and providing habitat for a rich range of biota (Callaway *et al*. 2012; Gibbs 2001). However, as little as 10% of California's historical wetland cover remains today (California Department of Fish and Wildlife 2001). This historic decrease in wetland cover is likely to worsen with the potential increased frequency of disturbances that further reduce and degrade wetland cover, especially continued sea level rise, coastal erosion, deposition, and anthropogenic marine debris (Doughty and Cavanaugh 2019; Tweel and Turner 2012; Uhrin and Schellinger 2011). To mitigate the impacts of disturbance, management should include the effects of disturbances in the understanding of healthy marsh form and function. For instance, sediment deposition is a common and important process in many marshes, with hurricane deposition being often studied and found to deliver

sediment important for nutrient delivery and the ability to offset sea level rise (Tweel and Turner 2012; Callaway *et al.* 2012). In contrast, anthropogenic marine debris, such as fishing gear and wooden poles, has been found to be detrimental to marshes by damaging plant structures if it remain for a length of time (Uhrin and Schellinger 2011), and oiling temporarily increases shoreline loss of effected wetlands (Beland *et al.* 2017).

The Montecito debris flows are a unique situation in the scope of prior literature. Debris flows are an episodic disturbance event; however, they are not one commonly studied, in which most research has focused on oiling, hurricanes deposition, or anthropogenic marine debris (Beland *et al.* 2017; Tweel and Turner 2012; Callaway *et al.* 2012; Uhrin and Schellinger 2011). Furthermore, many studies examining disturbance events in salt marshes have focused on the Gulf of Mexico and the east coast of the U.S. (Klemas 2013a, Klemas 2013b, Uhrin and Schellinger 2011, Beland *et al.* 2017, Tweel and Turner 2012; Peterson *et al.* 2015). However, the disturbances that are common in those regions, such as hurricanes, are not common on the west coast of the U.S., and the findings of these studies may not be fully applicable to debris flows. Thus, the question of how the Montecito debris flow impacted the marsh becomes of interest. However, addressing this question with field methods is complicated by the fact that the debris flow could not be predicted and that Carpinteria Salt Marsh Reserve is a highly managed system. The unpredictability of the event meant that there was not ample time to collect field observational data to assess conditions prior to the event. Furthermore, a combination of manager intervention and inundation by king tides— exceptionally high tides—removed sediment from the marsh and limited the ability to collect field data following the event. Remotely sensed data, however,

was collected before and following the event and could be used to assess impacts of the debris flow on the marsh.

Remote sensing, including change detection, biomass estimation, and land cover classification, is a common tool in the study of wetlands with a large range of uses and has often been used when ground data are scarce (Klemas 2013A; Rosso *et al.* 2005). Due to recent advancements in sensor design and data analysis, remote sensing is becoming more practical for monitoring natural and anthropogenic changes in coastal systems (Klemas 2013B) Prior studies have used a variety of sensors (e.g. Landsat, AVIRIS, LiDAR, Planetscope, and drone data), techniques (e.g. maximum likelihood classification, MESMA, reclassification, random forest, and post-classification change detection), and indices (e.g. normalized difference vegetation index) to monitor coastal wetland conditions—some of which made recommendations for best approaches to wetland remote sensing (Klemas 2013A; Miller *et al.* 2019; Eastwood *et* al. 1997; Doughty and Cavanaugh 2019; Beland *et al*. 2017; Peterson *et al.* 2015; Wu *et al.* 2020; Nasser Mohamed Eid *et al*. 2020; Parihar *et al*. 2012). These sensor and index recommendations vary depending on the wetland type and the characteristics that are being assessed. Index recommendations are more dependent on the type of wetland being assessed. For example, one study recommended the use of the modified soil adjusted vegetation index (MSAVI) and global environmental monitoring index (GEMI) for intertidal marshes (Eastwood *et* al. 1997). However, another study recommended the normalized difference vegetation index (NDVI) and the green normalized difference vegetation index (GNDVI) for global wetland assessment and two others for woody forested wetlands specifically (Taddeo *et al*. 2019).

Unlike indices, techniques and sensors used to assess wetland cover and characteristics can often be built on each other. One study implemented the use of fractional cover of different endmembers obtained by spectral mixture analysis (SMA) and multiple endmember spectral mixture analysis (MESMA; Roberts *et al.* 1998) in the classification of a marsh in the southern San Francisco Bay (Rosso *et al.* 2005). While both approaches have challenges, MESMA was found to provide a more accurate representation of fractional cover, especially if 4- or 5-endmember models were used with more than one endmember per class (Rosso *et al*. 2005). Peterson *et al.* (2015) used MESMA on advance visual/infra-red imaging spectrometer (AVIRIS) data to detect oil-impacted regions of coastal salt marsh with high accuracy (87.5% to 93.3%). Beland *et al.* (2017) was then able to use these oil maps and image change analysis to determine that oiling temporarily accelerated land loss in coastal marshes. These studies highlight the effectiveness of MESMA as a technique for classifying wetland landcover and detecting areas affected by disturbance.

Other classification methods have also been used for tracking change. For example, one study used NDVI to track vegetation colonization in Petaluma River Marsh after tidal restoration via post-classification change detection and concluded that NDVI can be used to differentiate vegetated and non-vegetated portions of marshes and is robust to human interpretations of NDVI (Tuxen *et al*. 2008). Another study used Breaks For Seasonal and Trend (BFAST) and random forest classification on monthly Landsat NDVI products to perform change detection in forested wetlands with a classification accuracy of 92.96% and change detection accuracy of 87.8% (Wu *et al.* 2020). Parihar *et al*. (2012) used maximum likelihood classification on Landsat MSS and TM data sets to track changes in the East Kolkata Wetlands in the absence of ground data, though accuracy of this method was

between 73.80% and 79.33%. Im *et al*. (2008) also showed that high point density LiDAR data can be used for object-based land cover classification with high accuracies (> 90%) without the need for incorporating additional remote sensing data. Each of these papers highlights the effectiveness of different methods and data inputs on accurately classifying landcover.

Based on the recommendations and results of other studies, the approach taken here is post-classification change detection on a short time series of remotely sensed images classified by a random forest classifier with the aim of identifying effects on marsh landcover following the Montecito debris flow.

II. Methods

A. Site Description

Figure 1: Carpinteria Salt Marsh outlined with study extent (NAIP Imagery, USDA, 2018)

The ecosystem of interest for this study is Carpinteria Salt Marsh Reserve (CSMR), located in Carpinteria, CA (34.4012° N, 119.5379° W) situated between California Highway 101, downtown Carpinteria, and the Pacific Ocean (Figure 1). CSMR is divided into three sections, the largest of which is managed by University of California, Santa Barbara (UCSB) as part of the University of California (UC) Natural Reserve System (Brooks 2019, personal communication). The wetland is a heterogeneous landscape made up of 93 hectares of annual and perennial herbs and grasses, transitional upland habitat, water channels, and mud flats ranging between -1 to 3 m above sea level (Doughty and Cavanaugh 2019). The plant community can be split into two categories: mid marsh, primarily dominated by *Salicornia pacifica* (formerly *Salicornia virginica*, pickleweed), and high marsh, which is a mix of *Salicornia pacifica, Jaumea carnosa* (marsh jaumea), *Distichlis littoralis* (shore grass), *Arthrocnemum subterminale* (Parish's glasswort), *Frankenia salina* (alkali heath), and a few other less abundant species (Doughty and Cavanaugh 2019; Myers *et al.* 2017). Water inputs come largely from tidal inundation and water inlets in the eastern portion of the marsh that allow for input from further inland (Brooks 2019, personal communication).

B. Data Description and Correction

The imagery used in this study is Sentinel-2 A and B data produced by the European Space Agency. The mission is composed of twin wide swath, high-resolution, multispectral satellites that have a revisit frequency of five days using both sensors. Both satellites carry optical sensors that sample in 13 spectral bands at varying spatial resolutions (European Space Agency n.d.; Drusch *et al*. 2012). The high temporal resolution of the two satellites allowed the assembling of a good time series for quantifying marsh changed despite the variable cloud cover and inundation of the CSMR. Dates were selected to represent similar

times of year, tide, and cloud cover. Four dates were selected to highlight pre-flow, immediate, and two post-flow conditions (approximately one and three years after the initial event). November 13, 2017 imagery was used for pre-flow as it was the data closest to the debris flow in which the marsh was not flooded or covered by clouds. January 12, 2018 imagery represents the post-flow conditions as the data were collected three days after the flow occurred and before mechanical clean up and king tides occurred. Lastly, November 3, 2018 and November 12, 2020 imagery represent two recovery steps and were chosen to be consistent with the pre-flow November image. No November 2019 imagery was selected, as all images available were collected when there was either dense cloud cover or the marsh was inundated by high tide. All Sentinel-2 imagery was downloaded from the USGS Earth Explorer portal (U.S. Geological Survey).

Imagery was preprocessed in Sentinel Application Platform (SNAP) prior to being implemented in ENVI Classic 5.5.3 (SNAP; Harris Geospatial). First, the Sen2Cor SNAP add-on was used to perform atmospheric correction to obtain bottom of atmosphere L2A imagery from the top of atmosphere L1C imagery downloaded from the USGS (Main-Knorn *et al.* 2017). This process produced 12 atmospherically corrected L2A bands. Once corrected, bands 1, 9, and 10 were removed as they primarily are used for atmospheric properties and are too coarse (60 m resolution) to be used in assessment of the fine scale change in the marsh. The remaining 20 m resolution bands (bands 5, 6, 7, 8A, 11, and 12) were then resampled using pixel replication to match the 10 m resolution of bands 2, 3, 4, and 8. Resampled and native 10 m resolution bands were layer stacked for further processing in ENVI.

High density LiDAR was also used in addition to Sentinel-2 imagery to assess conditions immediately after the debris flows occurred (January 2018). LiDAR data were collected over the areas affected by the debris flows soon after the event by the Federal Emergency Management Agency (FEMA) at a density of at least 4 points per square meter (Federal Emergency Management Agency 2018). LiDAR data were corrected and processed using the BCAL add-on for ENVI (Harris Geospatial; BCAL Lidar Tools). Data were height filtered at a threshold of 30m with a 10m search window. Height filtered data were then processed using last returns into a digital terrain model (DTM) with 10m resolution to match Sentinel-2 data.

C. Spectral Analysis

Before classification, corrected Sentinel-2 images were processed to obtain fractional cover, and to calculate the normalized difference vegetation index (NDVI)and modified anthocyanin reflectance index (mARI).

Fractional cover was obtained via MESMA using the following steps. First, two spectral libraries were generated using the November 2017 and January 2018 processed images. Endmembers were selected based on site knowledge and similarity of spectra to those that would be expected for each landcover class (Figure 2). Both libraries had endmembers selected to represent four broad landcovers that are expected in the marsh: non-photosynthetic vegetation (NPV), green vegetation, bare soil, and subtidal. Libraries were then optimized using the endmember average RMSE (EAR)/minimum average spectral angle (MASA)/count based endmember selection (CoB) (EMC; Dennison and Roberts 2003; Dennison *et al.* 2004; Roberts *et al.* 2003) option in VIPER Tools and included a minimum of four endmembers per endmember class (Roberts *et al.* 2019). The November

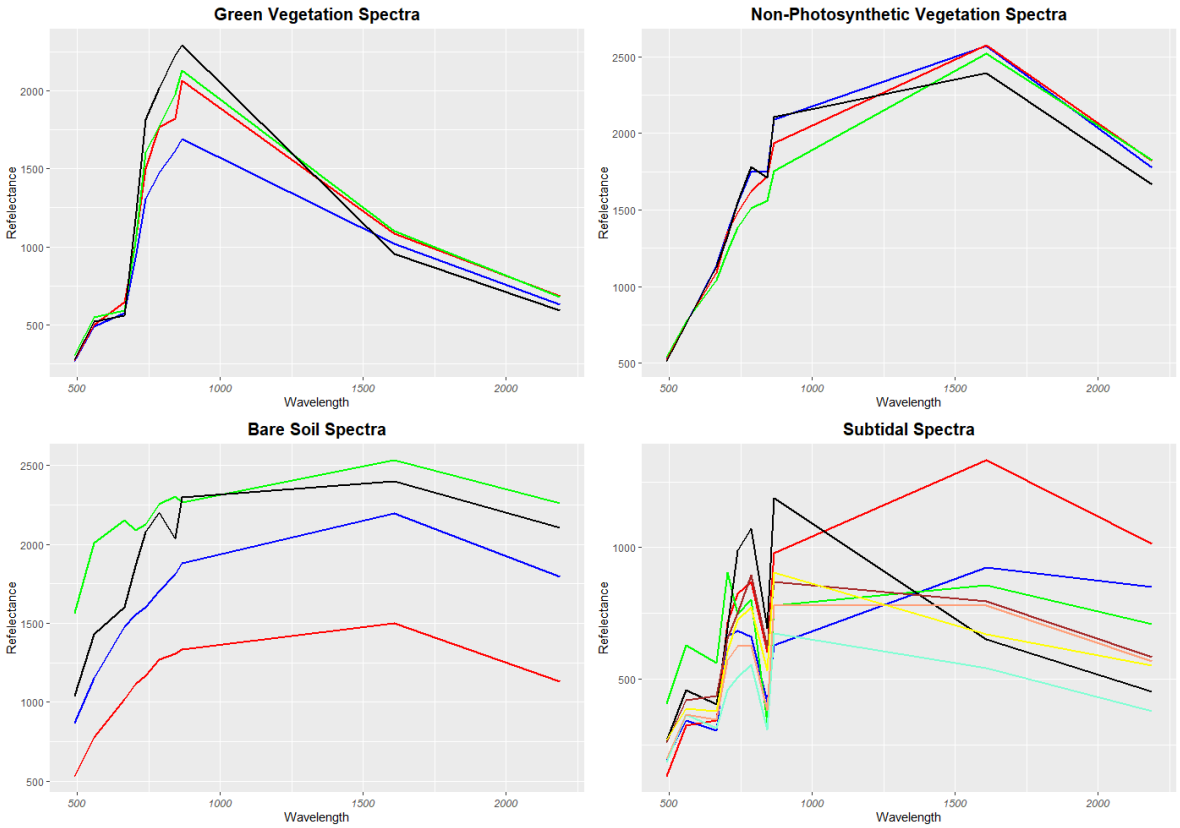

Figure 2: Spectral library for November 2017. Axes are (x) wavelength in nm and (y) reflectance values. A) non-photosynthetic vegetation spectral signatures, B) green vegetation spectral signatures, C) bare soil spectral signatures, D) subtidal spectral signatures. January spectra included in Appendix B.

library was used for the pre-debris and two recovery images. The January 2018 image had a separate spectral library for the unique conditions that were expected around the debris flow.

With the libraries generated, MESMA was then performed to obtain fractional cover for all four dates. Endmember models used were 2, 3, 4, and 5-endmember models to ensure the inclusion of the model approaches recommended by Rosso *et al*. (2005). All models were constrained to fractional cover between 0.0 and 1.0, shade fraction between 0.0 and 0.8, and a maximum root mean square error of 0.025. This process produced fractional cover for the four endmember classes (Figure 3).

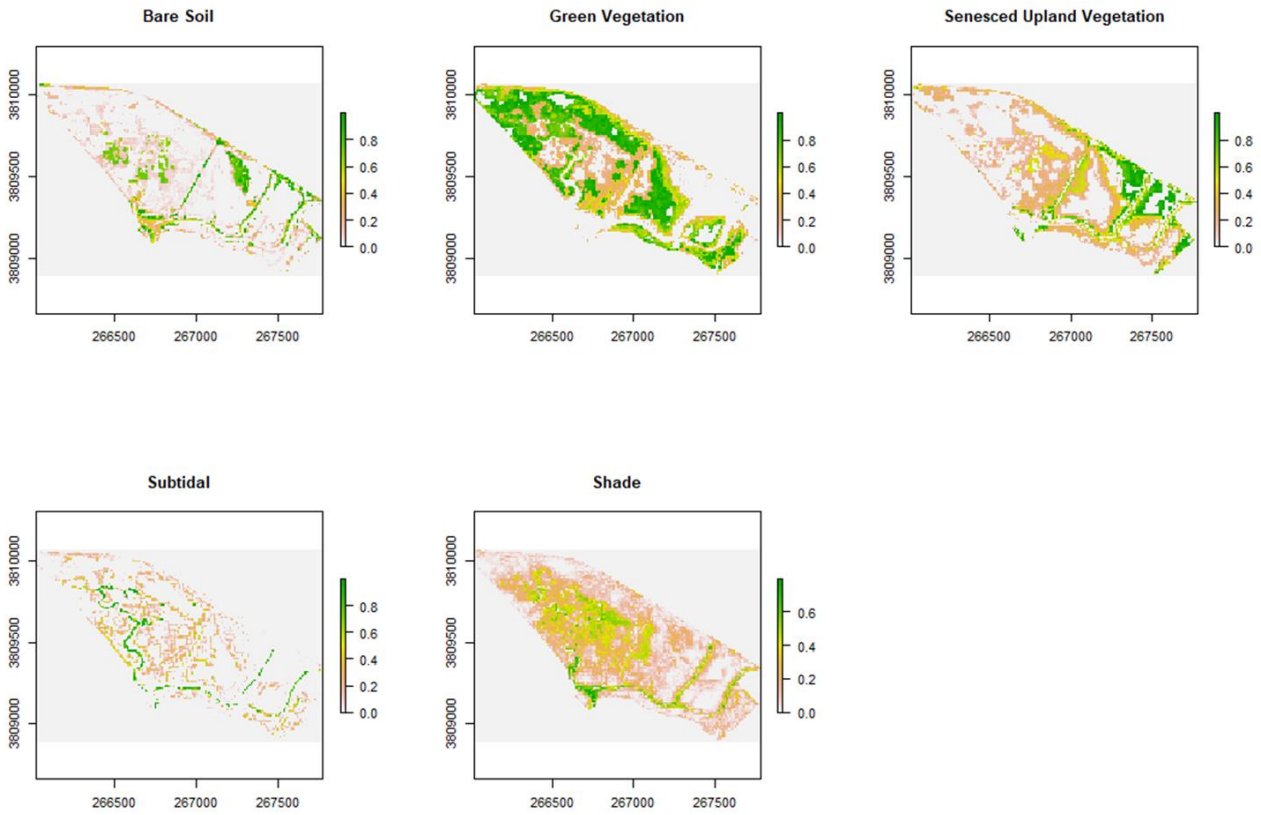

Figure 3: An example of fractional cover in November 2020. Scale indicates proportion of pixel that is made up of respective endmembers or shade.

To further build on the data that would guide the classification of CSMR, two vegetation indices were calculated from the Sentinel-2 imagery: NDVI (eq.1; Rouse *et al,* 1974) and mARI (eq.2; Gitelson *et al*. 2006; Gitelson *et al.* 2009).

$$NDVI = \frac{NIR - RED}{NIR + RED} = \frac{Band\ 8 - Band\ 4}{Band\ 8 + Band\ 4} \quad Eq.1$$

NDVI is one of the vegetation indices recommended in the literature for wetland analysis and was found to be one of the more important factors in classifying landcover classes in CSMR in prior work (Klemas 2013; Tuxen *et al*. 2008, Doughty and Cavanaugh 2019, Silva 2020).

$$mARI = 800\text{nm} * \left(\frac{1}{550\text{nm}} - \frac{1}{700\text{nm}}\right) = \text{Band } 8 * \left(\frac{1}{\text{Band } 3} - \frac{1}{\text{Band } 5}\right) \quad Eq.2$$

mARI is used to detect the levels of anthocyanins, a family of red pigments that can be related to stress and senescence in plants (Gitelson *et al*. 2001). Anthocyanin content in *Salicornia pacifica* has been found to increase in the fall and winter (Farrens 1971). Therefore, the mARI has the potential to further help the classification of both senesced vegetation and a dominant marsh plant in CSMR.

The last step was training data generation. Once the Sentinel-2 and LiDAR products were produced, data were layer stacked prior to the creation of training data. Training data were produced for five landcover classes—bare soil, high marsh, mid marsh, senesced, and subtidal—by selecting reference polygons that matched regions of corresponding landcover from an expert map and report of landcover prior to the debris flow and additional interpretation of layer values as seen in Table 1 (Myers *et al*. 2017). The high marsh class

Table 1: Training Data Parameters

Training Data					
Class	***Polygon Count***				***Metric***
	Nov-17	Jan-18	Nov-18	Nov-20	
Bare soil	10	11	17	13	High Bare Soil Fractions, Low NDVI, Low mARI
High Marsh	5	5	10	7	High Green Vegetation Fractions, High NDVI, High mARI
Mid Marsh	12	7	16	13	Moderate-High NDVI, Mixed Green Vegetation Fractions and Bare Soil Fractions
Senesced	8	5	8	5	High Non-photosynthetic Vegetation Fractions, Low NDVI, Moderate-High mARI
Subtidal	20	7	21	19	High Subtidal Fractions, Low NDVI, Low mARI, Channels where expected

represents a mixed plant community of *Salicornia pacifica, Arthrocnemum subterminale, Frankenia salina,* and *Distichlis spicata*. Mid marsh represents portions of the marsh dominated by by *S. pacifica*. The senesced landcover is composed of upland regions dominated by non-native shrubs and grasses (Myers *et al.* 2017). Training data were collected for each date by creation of rectangular polygons in ArcGIS (Environmental Systems Research Institute; Table 1). Training data and layer stacked images were then analyzed in R (R Core Team 2019; Code included in Appendix A).

D. Random Forest and Change Detection

Classification was done via a random forest classifier. Random forest is a machine learning technique that automates the categorization of data by running a datapoint (e.g. a pixel) through a set number of decision trees and picking a finalized landcover class via majority vote. Pixel values were first extracted from the layer stacked images with the values and associated landcover recorded into a data frame, which was then filtered to remove variables with NA/NULL values. The data frame was then read into the random forest algorithm, with n=500 decision trees. This process produced classified maps of the five landcover classes. Additional outputs include variable importance, a measure that identifies which layer stack inputs were important in the landcover classification, mtry accuracy and kappa values, an accuracy assessment of the training data, and out of bag (OOB) error. Final results were resampled in R and accuracy values averaged to perform a k-fold cross validation.

Post-classification change detection was performed in ENVI using the change detection statistics option. Dates were compared to each other in both chronological order (i.e. November 2017 to January 2018, November 2018 to November 2020) and net order

(November 2017 to November 2020). Comparing the dates this way allowed for tracking of landcover extent for all 5 classes as time progressed and obtaining net change for each landcover in the system. ENVI output change statistics in terms of pixel count, area in square meters, and percentage change. These statistics include class differences and image differences. Percentage change was recalculated using both pixel count and area and used in place of the ENVI reported percentages.

III. Results

A. Random Forest

Variable importance was used to determine which of the random forest inputs were most important in the landcover classification of CSMR. Variable importance was measured by the mean decrease in Gini index, a measure in which higher values indicate higher importance in the model (Lee 2017). From this measure, NDVI and green vegetation fraction were the most important variables in three of the four years. NDVI and green vegetation fractions did not have the highest importance in January 2018 and November 2020, respectively. Secondary variables that also had high importance were mARI, bare soil fractions, and senesced vegetation. mARI had greater importance in the recovery timesteps compared to the earlier dates. Shade fractions and subtidal fractions had the lowest amount of importance in the majority of the dates. The bare surface model (digital elevation) was only available in January 2018 but had moderate importance in the model.

Overall accuracy of the random forest classification across all dates was measured by mtry, OOB error, and k-fold cross-validation. Mtry indicates the number of splits that occur at each node within a decision tree; the random forest model then selects the mtry with the

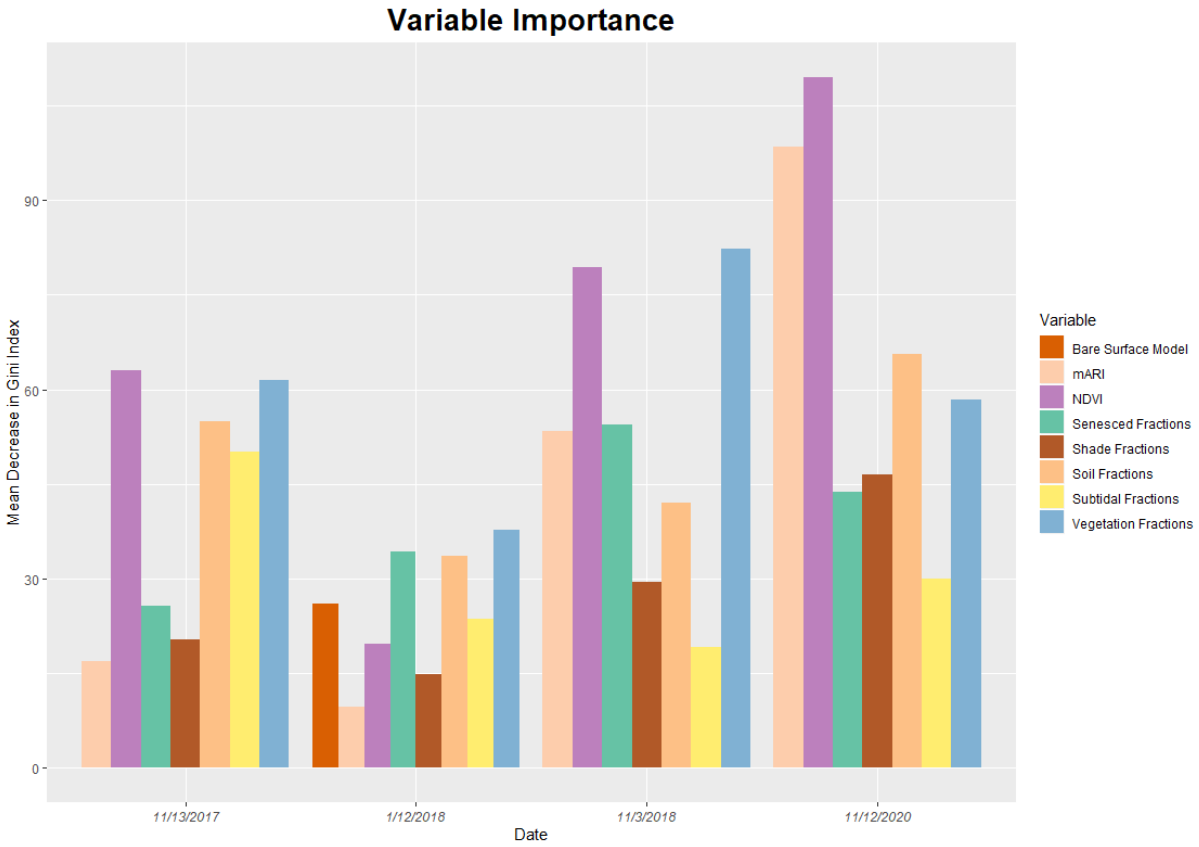

Figure 4: Variable importance measured by mean decrease in Gini Index, higher values indicate higher importance in random forest classification. NDVI and green vegetation fractions frequently had the highest importance. Variables appear in alphabetical order. Note: bare surface model/digital elevation model was only used for Jan 2018.

highest accuracy as the final prediction. Mtry accuracy (mtry= 2, 5, 2, and 2 respectively, Table 1) values were high for all four dates—0.994, 0.920, 0.956. and 0.963, respectively—with similar kappa values—0.993, 0.897, 0.956, 0.953. However, these values may be overpredicted as they are generated from within the training data.

OOB error and k-fold cross validation are secondary accuracy measures used to confirm accuracy from mtry. OOB error measures prediction error of random forests using bootstrap aggregating and is recalculated as more trees are added to the random forest model. OOB error rates agree with mtry accuracy and indicate high accuracy values of the

Table 2: Training Data Accuracy Tables

Nov. 17 Training Data Pixels							
	Bare Soil	High Marsh	Mid Marsh	Senesced	Subtidal/Water	**Total (Pixels)**	***User's Error***
Bare Soil	*49*	0	2	0	0	**51**	***0.03921569***
High Marsh	0	*112*	0	0	0	**112**	***0***
Mid Marsh	0	0	*80*	0	0	**80**	***0***
Senesced Veg.	0	0	1	*55*	0	**56**	***0.01785714***
Subtidal/Water	0	0	0	0	*79*	**79**	***0***
Total (Pixels)	**49**	**112**	**83**	**55**	**79**	**378**	
Producer's Error	***0***	***0***	***0.036144578***	***0***	***0***		
	mtry						
	mtry	Accuracy	Kappa	AccuracyS	KappaSD		
1	**2**	**0.9944266**	**0.9928624**	**0.006473**	**0.008277264**		
2	4	0.9889336	0.9858201	0.010455	0.013348661		
3	7	0.9804847	0.9750409	0.014986	0.019107141		

Jan. 18 Training Data Pixels							
	Bare Soil	High Marsh	Mid Marsh	Senesced	Subtidal/Water	**Total (Pixels)**	***User's Error***
Bare Soil	*78*	0	1	0	0	**79**	***0.01265823***
High Marsh	0	*59*	1	0	0	**60**	***0.01666667***
Mid Marsh	3	2	*34*	0	2	**41**	***0.17073171***
Senesced Veg.	0	0	0	*47*	0	**47**	***0***
Subtidal/Water	1	1	4	0	*24*	**30**	***0.2***
Total (Pixels)	**82**	**62**	**40**	**47**	**26**	**257**	
Producer's Error	***0.04878***	***0.0483871***	***0.15***	***0***	***0.076923077***		
	mtry						
	mtry	Accuracy	Kappa	AccuracyS	KappaSD		
1	2	0.9172968	0.8930668	0.020359	0.02645464		
2	**5**	**0.9203775**	**0.8970671**	**0.025751**	**0.03328449**		
3	8	0.9154432	0.8907413	0.025699	0.03303982		

Table 2 (cont.): Training Data Accuracy Tables

Nov. 18 Training Data Pixels							
	Bare Soil	High Mars	Mid Marsh	Senesced	Subtidal/Water	**Total (Pixels)**	***User's Error***
Bare Soil	*61*	0	4	3	0	**68**	***0.10294118***
High Marsh	0	*149*	0	0	0	**149**	***0***
Mid Marsh	2	0	*129*	0	2	**133**	***0.03007519***
Senesced Veg.	1	0	0	*52*	0	**53**	***0.01886792***
Subtidal/Water	2	0	5	1	*67*	**75**	***0.10666667***
Total (Pixels)	**66**	**149**	**138**	**56**	**69**	**478**	
Producer's Error	***0.075758***	***0***	***0.065217***	***0.071429***	***0.028985507***		
	mtry						
	mtry	Accuracy	Kappa	AccuracySD	KappaSD		
1	**2**	**0.956424**	**0.943175**	**0.012944**	**0.01645829**		
2	4	0.95145	0.936647	0.013118	0.01679813		

Nov. 20 Training Data Pixels							
	Bare Soil	High Mars	Mid Marsh	Senesced	Subtidal/Water	**Total (Pixels)**	***User's Error***
Bare Soil	*77*	0	1	1	3	**82**	***0.06097561***
High Marsh	0	*173*	1	0	0	**174**	***0.005747126***
Mid Marsh	0	1	*119*	0	6	**126**	***0.055555556***
Senesced Veg.	0	0	0	*107*	0	**107**	***0***
Subtidal/Water	0	0	6	0	*92*	**98**	***0.06122449***
Total (Pixels)	**77**	**174**	**127**	**108**	**101**	**587**	
Producer's Error	***0***	***0.005747***	***0.062992***	***0.009259***	***0.089108911***		
	mtry						
	mtry	Accuracy	Kappa	AccuracySD	KappaSD		
1	**2**	**0.96322**	**0.953061**	**0.011581**	**0.01481611**		
2	4	0.958653	0.947234	0.012874	0.01651967		
3	7	0.944668	0.929458	0.01555	0.01970101		

random forest classifications (OOB= 0.008, 0.074, 0.044, 0.031, for Nov. 2017, Jan. 2018, Nov. 2018, and Nov. 2020, respectively). K-fold cross validation is a validation technique in which data were iteratively resampled *k*-times, and prediction error or accuracy is averaged among all iterations (Brinberg n.d.). Data were resampled using the default iterations (*k*=25) in R and averaged to obtain accuracy rates for all dates. As with OOB error, k-fold cross validation showed agreement with mtry accuracy and provides further evidence that the results of the random forest classifier have a high degree of accuracy (k-fold value = 0.993, 0.910, 0.957, 0.962).

Landcover class accuracy was measured via producer's and user's error and allows for the assessment of the mapping of individual landcover classes. High marsh vegetation was

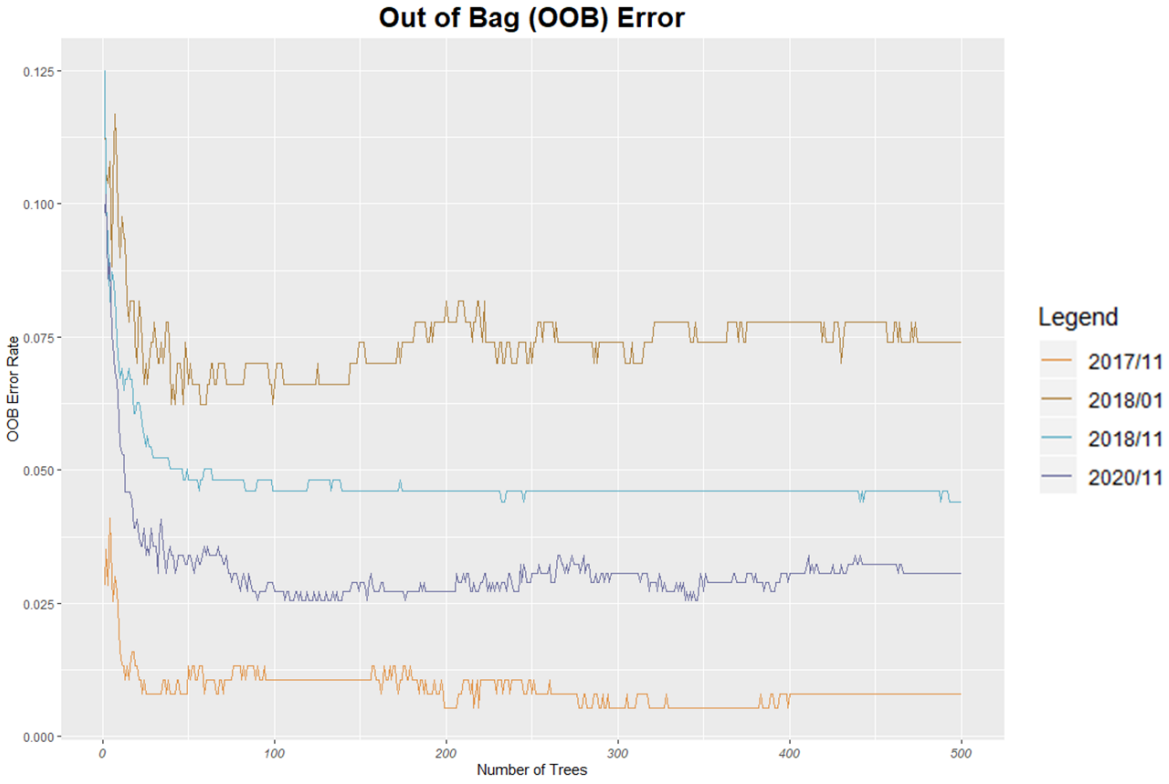

Figure 5: Out of bag (OOB) error graphs for the four random forest classifications. As more trees are added to the random forest, less error occurs in the classification. Order from top to bottom: January 2018, November 2018, November 2020, and November 2017.

the most accurately mapped with low user's and producer's error across all dates. Subtidal and mid marsh had the greatest amount of user and producer's error, especially in January 2018. Subtidal cover had the greatest confusion with mid marsh vegetation and bare soil, while mid marsh was confused with bare soil and subtidal. Error within these two classes was below 10% for most dates, and classification for the two classes remained relatively accurate.

B. Post-Classification Change Detection

The random forest classifier produced four landcover maps for CSMR (Figure 6). Each map shows the extent of the five landcover classes—bare soil, high marsh, mid marsh, senesced, and subtidal—and represent different states of disturbance and recovery. The high marsh landcover had the most area in November 2017 and January 2018, while in November 2018 and 2020 mid marsh was the largest landcover class. Senesced vegetation and subtidal landcover experienced little change compared to bare soil, high marsh, and mid marsh vegetation.

The post classification change detection shows that a 19.25 ha increase in bare soil coverage occurred between November 2017 and January 2018, amounting to 27.83 ha of the marsh being covered in bare soil immediately following the debris flow (Figure 7). In November 2020, bare soil coverage decreased by 16.59 ha (60%) since January 2018—a decrease of bare soil coverage to 11.24 ha (12%) of total marsh area—and resulting in a 2.66 ha (31%) net increase in bare soil coverage between November 2017 and November 2020. On the other hand, overall marsh vegetation (high marsh + mid marsh) coverage changed little with only a 0.12% net increase in total vegetation coverage between November 2017 and November 2020. However, when split into the two respective landcover classes, high

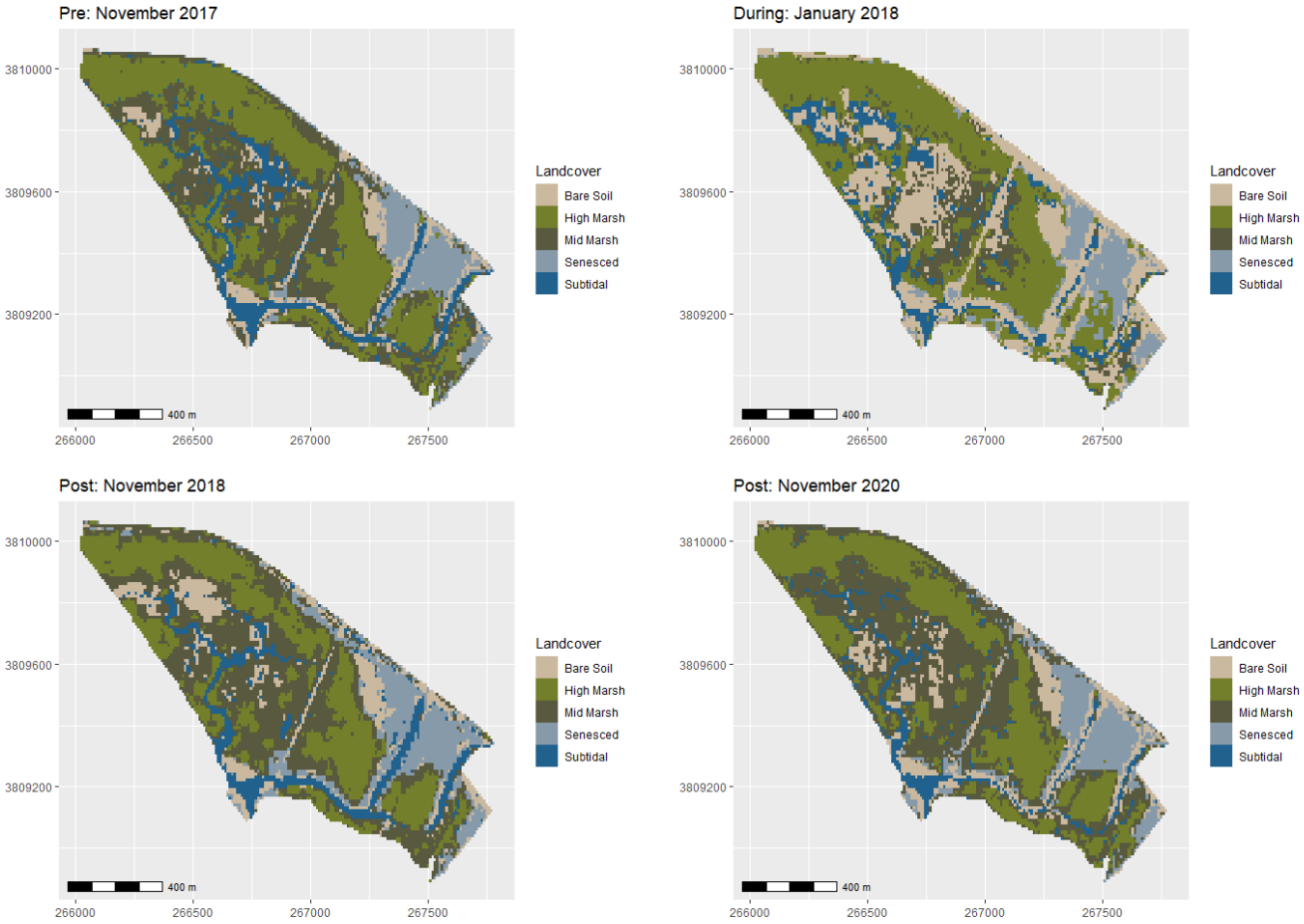

Figure 6: Maps produced by the random forest classification. Maps depict the extent of bare soil, high marsh, mid marsh, senesced vegetation, and subtidal/water landcover. Top to bottom, left to right: November 2017, January 2018, November 2018, and November 2020. Individual maps included in Appendix B.

marsh vegetation coverage decreased as mid marsh vegetation increased. There are a few areas that where change in landcover is prominently seen in the landscape. Areas that were high marsh vegetation and near areas impacted by bare soil changed to mid marsh vegetation. This change is prominent in the areas near the salt pan in the northeast (Figure 8 B) and some of the mudflat region in the western portion of the marsh (Figure 8 A & C).

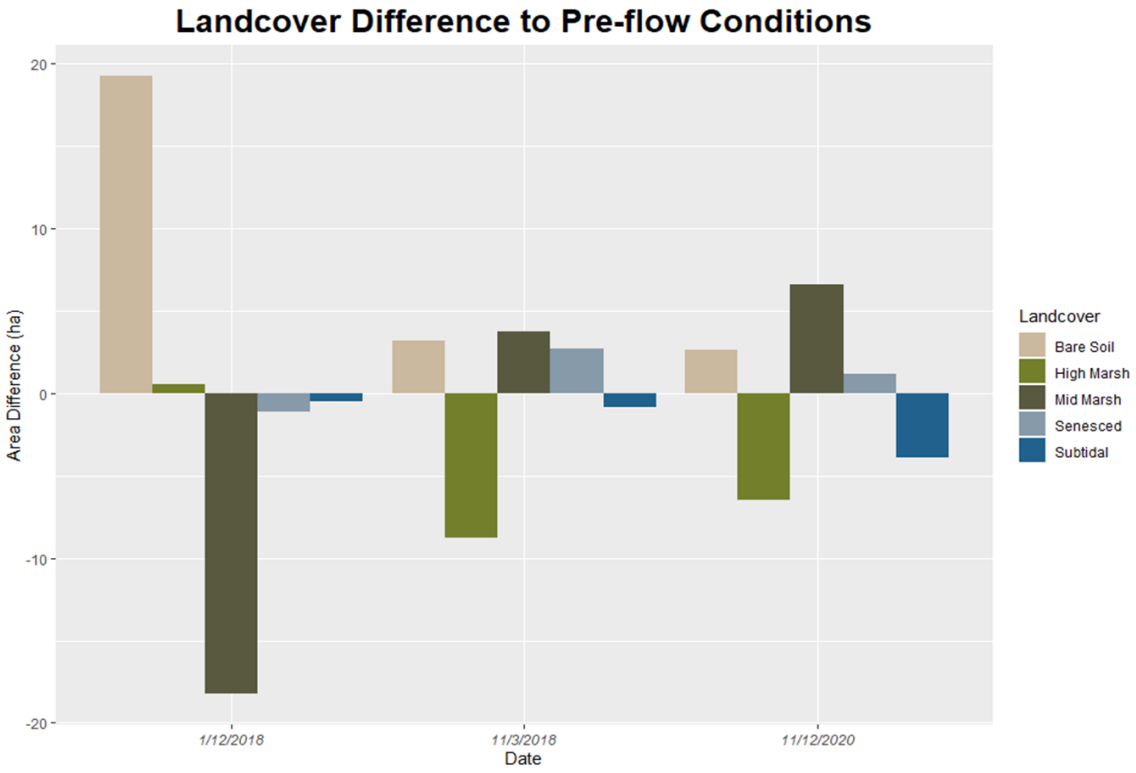

Figure 7: Difference of landcover class area (ha) compared to pre-flow conditions. Bars are clustered by date.

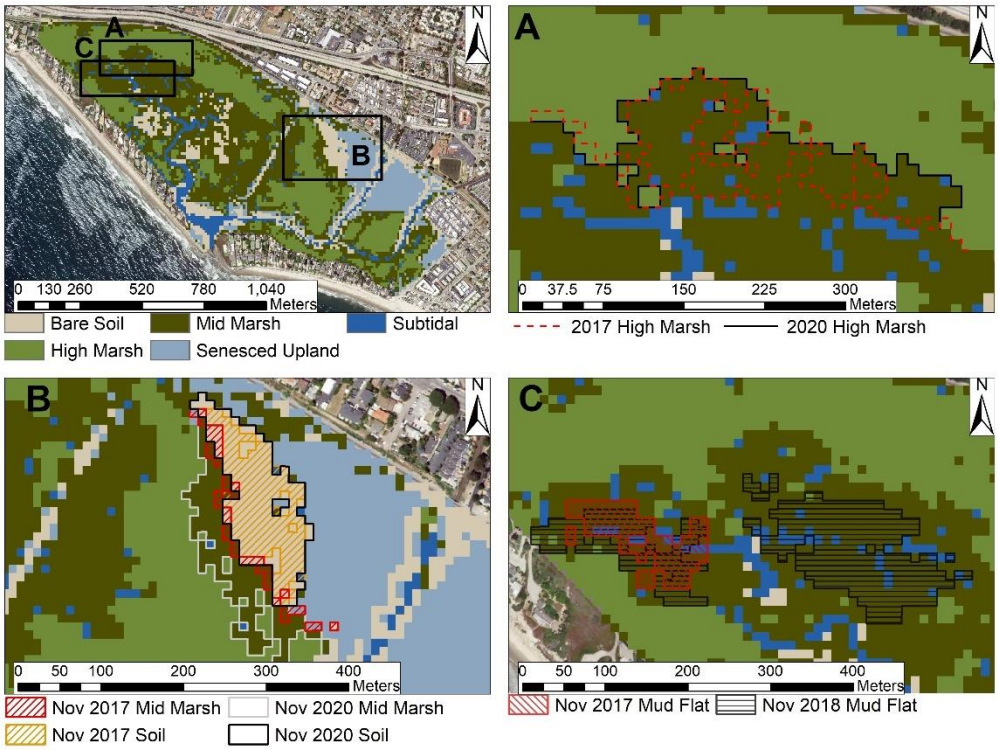

Figure 8: Maps highlighting areas where landcover change is most prominent. A) High marsh to mid marsh conversion, B) difference in salt pan and vegetated perimeter, C) difference in mudflat extent.

IV. Discussion

A. Variable Importance

The identification of important classification variables enables the identification of which landscape metrics are important in identifying landcover in the marsh from remote sensing imagery. As much of the landscape is either vegetated or covered in bare soil, variables that can be used to identify and classify these landcovers would be important metrics. Therefore, NDVI was likely used to differentiate mid and high marsh vegetation from the non-vegetation landcover classes, with bare soil fractions helping to differentiate the non-vegetated landcovers classes. Knowledge of variable importance could be useful in deciding which measurements to obtain when collection of field data is possible to combine with remotely sensed data. January 2018 had the lowest values for decrease in Gini index, and this could be linked to having more variables to use. However, this would have to be tested by adding elevation data of a similar quality to the other random forest classifications.

B. Accuracy Assessment

The three accuracy metrics (mtry, OOB error, and k-fold cross validation) suggest that landcover was accurately mapped by the random forest classifier and that the produced maps are reliable for use in change detection. The accuracy of the random forest classification is comparable to those of other studies. For example, Wu *et al*. (2020) also performed a random forest classification for a subtropical wetland that had a similar overall accuracy value of 0.9296 compared to this study's values of 0.994, 0.920, 0.956. and 0.963. The model also performed as well as or better than classifications done using other methods, such as maximum likelihood classification, Iso-cluster unsupervised classification, or

reclassification/recoding of vegetation indices (Tuxen *et al.* 2007; Nasser Mohamed Eid *et al*. 2020; Parihar *et al*. 2012). The random forest classification done here was more accurate than the maximum likelihood classification done by Parihar *et al*. (2012), an average accuracy of 0.958 vs 0.765, respectively. When compared to reclassification, the random forest did approximately the same or slightly better, with reclassification having accuracy values of 0.814 and 0.963 (Tuxen *et al.* 2007). Iso-cluster classification on NDVI did somewhat better than the random forest with accuracy values of 0.9730, 0.9750, 0.9760, and 0.9800 for the respective dates (Nasser Mohamed Eid *et al*. 2020).

High marsh had the highest accuracy, and we can be most sure of the mapping of this landcover class when compared to the other landcover classes. The mid marsh class had one of the highest user's and producer's errors. As mid marsh is one of the classes that experienced the most change following the debris flow, any error present in its classification presents a problem; however, this error only exceeds 10% in January 2018 (user's: 17%, producer's: 15%) and is within acceptable margins for all other dates. There are a few possible sources for the error observed: 1) training data may have included misclassified pixels and introduced error to the corresponding landcover class, 2) pixels may have had values similar to that of multiple landcover classes, 3) resampled 20 m resolution Sentinel-2 bands may have still been too coarse to assess changes in the marsh, and 4) the use of a different spectral library for January 2018 may have led to lower accuracies for this date. To remedy this, the use of data from higher spatial resolution sensors may be useful in reducing the frequency of mixed pixels and the need for fractional cover. Additionally, higher spectral resolution may improve the building of spectral libraries that can better differentiate between endmember classes, which then improves inputs into the random forest model.

C. Landcover Change and Ecological Implications

A majority of the landcover change occurred in bare soil, high marsh, and mid marsh vegetation. Bare soil area increased by 224% following the debris flows and dropped considerably in area by November 2018, likely due to the mechanical clean-up effort and king tides removing a large amount of the sediment. Bare soil continued to decrease until there was only a net 31% increase in bare soil by November 2020. This may indicate that the marsh is still recovering from the debris flows and continues to change over time.

Total vegetated area in the marsh seemingly showed little change over the 3 years with only a 0.12% increase in total marsh vegetation between November 2017 and November 2020. However, change is occurring, which is apparent when total vegetation is broken down into community types (high vs mid marsh) and compared. High marsh (a mixed community of *Salicornia pacifica, Arthrocnemum subterminale, Frankenia salina,* and *Distichlis spicata)* area decreased by about the same amount that mid marsh (primarily only *S. pacifica)* area increased, creating the illusion of little change in vegetated area. The post classification change detection showed that this shift from high to mid marsh community primarily occurred nearby changes in bare soil.

A change in the extent of community types may pose some ecological challenges that are important for salt marsh management and resilience, especially in areas where a change in extent means a reduction in biodiversity. The conversion to mid marsh vegetation from high marsh vegetation signifies a decrease in plant biodiversity as the community shifts from a mixed community to one that is largely composed solely of *S. pacifica*. A less diverse plant community may present a few management challenges. Studies have shown that a less diverse community is less resilient to the effects of disturbance, and spatial heterogeneity is

important in the enhancement of the resilience of ecosystem functions (Oliver *et al.* 2015). Less resilience may dictate a need for more management intervention following disturbances, especially as the frequency of disturbances, such as wildfire, sea level rise, and extreme weather, are predicted to increase with global climate change (Erwin 2009). Studies have found that the addition of sediment via depositional events can promote plant growth by the delivery of mineral nutrients (Tweel and Turner 2012). These nutrients may promote increased primary productivity by providing limiting nutrients. However, biodiversity has been found to be positively linked to primary productivity and its temporal stability (Oehri *et al.* 2017). A trend of conversion from a mixed community of several plant species to one made of primarily only one plant species may have harmful repercussions for marsh productivity and other ecosystem services and functions. Determining whether this change to a less diverse community is a permanent change or only a short-term intermediate step as the marsh recovers from the debris flow would require building up a longer time series of imagery over several years following the debris flows.

Sea level rise (SLR) is often considered a challenge for the conservation of coastal wetlands, especially in developed regions, as rising sea levels contribute to coastal squeeze, landcover change, fragmentation, and eventual loss of coastal marshes (Torio and Chmura 2013). Sediment deposition and soil accretion are viewed as important processes for the offsetting of SLR (Tweel and Turner 2012; Rosencranz *et al.* 2015). However, the results imply that debris flow deposition is also connected to landcover and plant community change. Therefore, landcover change may become an important consideration when planning for the management of coastal wetlands that can be prone to depositional events;

this study may become an important example of how to inform those plans in the absence of field data.

D. Limitations and Challenges

As discussed above, the resolution of remotely sensed data is important in the assessment of the fine scale changes that occur in marsh ecosystems. Some Sentinel-2 bands do not have a native 10m resolution and, therefore, have pixels that represent an average of a larger mix of landcover types. Resampling, as conducted in this study, only splits this coarser data into smaller pixels and not into its disaggregated components. Therefore, landcover classification would benefit from a sensor where all bands have the same fine spatial resolution. Baseline landcover prior to the debris flow was limited to a single date due to cloud cover, tide, and the length of historical record. Baseline assessments could be improved by using a sensor with a longer history or by using multiple dates per year. Ground truthing was also limited due to the lack of prior field data to compare against classification of historical imagery and due to the COVID-19 pandemic limiting ability to go into the field to collect such data, hence the emphasis on other accuracy metrics.

The results are also limited in their predictive power. For example, the rate at which sediment is being removed from the system or identification of whether the recently mapped sediment was the same sediment that had been deposited during the debris flow cannot be properly ascertained from these data. The exact process that leading to the conversion of high marsh to mid marsh vegetation also cannot be gauged from these data. It is also hard to make long term predictions from these results as the time series is short and the marsh is still experiencing change; therefore, it is difficult to conclude if the marsh will permanently convert to mid marsh or if this is only an intermediate step towards recovery.

V. Conclusion

The Montecito debris flows provided a unique opportunity to study debris interactions with marshes in a context different than what is known from previous studies which more commonly focused on hurricane deposition. This study used remote sensing to assess wetland response to this disturbance in the absence of field-based data. The method used here shows promise in being applied to other wetland systems. For example, the random forest model identified important classification variables that can be used to classify marsh landcover without field-based data. The method can also play an important first step in the identification of regions of interest that can be used to inform field campaigns to address further questions that arise from the use of remote sensing (e.g. a field campaign to assess the factors that are leading to the transition from high marsh to mid marsh vegetation). Data and information are an important part of making informed management decisions, and this study provides a successful demonstration of the use of post-classification change detection to assess wetland landcover response to an episodic event and the data that can be expected from such an assessment.

Post-classification change detection tracked change of the different landcover types in CSMR and found that mid marsh, high marsh, and bare soil landcover changed the most in the dates studied. Total marsh vegetation (high marsh + mid marsh) cover returned to similar levels to those before the debris flows; however, assessing change as total marsh vegetation, as was the initial frame of the research question, does not provide the proper conclusion. Areas that were covered in debris transitioned from high marsh vegetation to mid marsh vegetation, despite total vegetated area remaining relatively unchanged, which may be indicative of a process not captured in the scope of this study. Additionally, the results

suggest that the increase in bare soil coverage is potentially left over from the debris flow and may continue to slowly decrease over time via continued inundation or as plant communities recover. Carpinteria Salt Marsh is still changing, and the ecological implications of these changes are important considerations for wetland managers going into the future.

References

Andone, Dakin. 2018. “The Largest Wildfire in California’s Modern History is Finally Out, More Than 6 Months After It Started.” CNN. Cable News Network. https://www.cnn.com/2018/06/02/us/thomas-fire-officially-out/index.html.

BCAL LiDAR Tools. Idaho State University, Department of Geosciences, Boise Center Aerospace Laboratory (BCAL), Boise, Idaho. http://bcal.geology.isu.edu/envitools.shtml

Beland, Michael, Trent W. Biggs, Dar A. Roberts, Seth H. Peterson, Raymond F. Koklay, Sarai Piazza. 2017. “Oiling Accelerates Loss of Salt Marshes, Southeastern Louisiana.” *PLoS ONE* 12 (8). https://doi.org/10.1371/journal.pone.0181197

Brinberg, Miriam. n.d. “Cross-Validation Tutorial.” Cross-Validation Tutorial | QuantDev Methodology. QuantDev. Accessed June 8, 2021. https://quantdev.ssri.psu.edu/tutorials/cross-validation-tutorial.

Brooks, Andrew. 2019. (Director, Carpinteria Salt Marsh Reserve), in discussion with the author. October.

California Department of Fish and Wildlife. 2001. “Coastal Wetlands-Emergent Marshes.” California’s Living Marine Resources: A Status Report. https://nrm.dfg.ca.gov/FileHandler.ashx?DocumentID=34250

Callaway, John C., E.L Borgnis, R.E. Turner, and C.S. Milan. 2012. “Carbon Sequestration and Sediment Accretion in San Francisco Bay Tidal Wetlands." *Estuaries and Coasts* 35, 1163–1181. https://doi.org/10.1007/s12237-012-9508-9

Dennison, Phillip E. and Dar A. Roberts. 2003. “Endmember Selection for Multiple Endmember Spectral Mixture Analysis using Endmember Average RSME.” *Remote Sensing of Environment* 87: 123-135.

Dennison, Philip .E., K.Q. Halligan, and D.A. Roberts. 2004. “A Comparison of Error Metrics and Constraints for Multiple Endmember Spectral Mixture Analysis and Spectral Angle Mapper.” *Remote Sensing of Environment* 93: 359-367.

Doughty, Cheryl .L. and K.C. Cavanaugh. 2019. “Mapping Coastal Wetland Biomass from High Resolution Unmanned Aerial Vehicle (UAV) Imagery.” *Remote Sensing* 11, 540-556.

Drusch, Matthias, U. Del Bello, S. Carlier, O. Colin, V. Fernandez, F. Gascon, B. Hoersch, C. Isola, P. Laberinti, P. Martimort, A. Meygret, F. Spoto, O. Sy, F. Marchese, and P. Bargellini. 2012. “Sentinel-2: ESA's Optical High-Resolution Mission for GMES Operational Services.” *Remote Sensing of Environment* 120: 25-36. https://doi.org/10.1016/j.rse.2011.11.026.

Eastwood, J.A., M. G. Yates, A. G. Thomson, and R. M. Fuller. 1997. “The Reliability of Vegetation Indices for Monitoring Saltmarsh Vegetation Cover.” *International Journal of Remote Sensing* 18 (18): 3901-3907. DOI: 10.1080/014311697216739

Environmental Systems Research Institute. 2019. ArcGIS. Version 10.7.1. Redlands, CA. Environmental Systems Research Institute, Inc.

Erwin, Kevin. 2009. “Wetlands and Global Climate Change: The Role of Wetland Restoration in a Changing World.” *Wetlands Ecology and Management* 17: 71-84. DOI 10.1007/s11273-008-9119-1

European Space Agency. n.d. “Overview – Sentinel Online.” https://sentinel.esa.int/web/sentinel/missions/sentinel-2/overview

Farrens, Gary. 1971. *Color Change and Succulence in* Salicornia pacifica, Master’s Thesis, San Jose State University, San Jose.

Federal Emergency Management Agency. 2018. Montecito Debris Flow LiDAR [Data file]. Provided by Kristen Morell, faculty in UCSB Department of Earth Science.

Gibbs, James P. 2000, “Wetland Loss and Biodiversity Conservation.” *Conservation Biology* 14, 314-317. https://doi.org/10.1046/j.1523-1739.2000.98608.x

Gitelson, Anatoly A., Mark N. Merzlyak, and Olga B. Chivkunova. 2001. “Optical Properties and Nondestructive Estimation of Anthocyanin Content in Plant Leaves.” *Photochemistry and Photobiology* 74, 38-45. https://doi.org/10.1562/00318655(2001)074<0038:OPANEO>2.0.CO;2

Gitelson, Anatoly A., Galina P. Keydan, and Mark N. Merzlyak. 2006. "Three-Band Model for Noninvasive Estimation of Chlorophyll Carotenoids and Anthocyanin Contents in Higher Plant Leaves" *Geophysical Research Letters* 33. doi:10.1029/2006GL026457

Gitelson, Anatoly A., Olga B. Chivkunova, and Mark N. Merzlyak. 2009. “Non-Destructive Estimation of Anthocyanins and Chlorophylls in Anthocyanic Leaves.” *American Journal of Botany* 96 (10): 1861-1868. doi:10.3732/ajb.0800395

Harris Geospatial. “Exelis Visual Information Solutions.” Boulder, Colorado

Im, Jungho, John R. Jensen, and Michael Hodgson. 2008. “Object-Based Land Cover Classification Using High-Posting-Density LiDAR Data.” *GIScience & Remote Sensing* 45 (2): 209-228. DOI:10.2747/1548-1603.45.2.209

Kean, J.W., D.M. Staley, J.T. Lancaster, F.K. Rengers, B.J. Swanson, J.A. Coe, J.L. Hernandez, A.J. Sigman, K.E. Allstadt, and D.N. Lindsay. 2019. “Inundation, Flow Dynamics, and Damage in the 9 January 2018 Montecito Debris-Flow Event, California, USA: Opportunities and Challenges for Post-Wildfire Risk Assessment.” *Geosphere* 15 (4): 1140–1163. https://doi.org/10.1130/GES02048.1.

Klemas, V. 2013A. “Remote Sensing of Coastal Wetland Biomass: An Overview.” *Journal of Coastal Research* 29 (5): 1016– 1028.

Klemas, V. 2013B “Remote Sensing of Emergent and Submerged Wetlands: An Overview.” *International Journal of Remote Sensing* 34 (18): 6286-6320. DOI: 10.1080/01431161.2013.800656

Lee, Ceshine. 2017. “Feature Importance Measures for Tree Models — Part 1.” https://medium.com/the-artificial-impostor/feature-importance-measures-for-tree-models-part-i-47f187c1a2c3

Main-Knorn, Magdalena, Bringfried Pflug, Jerome Louis, Vincent Debaecker, Uwe Müller-Wilm, and Ferran Gascon. 2017. “Sen2Cor for Sentinel-2.” 3. 10.1117/12.2278218.

Miller, G. J., J. T. Morris, and C. Wang. 2019. “Estimating Aboveground Biomass and Its Spatial Distribution in Coastal Wetlands Utilizing Planet Multispectral Imagery.” *Remote Sensing* 11, 2020-2036.

Myers, M. R., D. R. Cayan, S. F. Iacobellis, J. M. Melack, R. E. Beighley, P. L. Barnard, J. E. Dugan, and H. M. Page. 2017. *Santa Barbara Area Coastal Ecosystem Vulnerability Assessment*. CASG-17-009. California.

Nasser Mohamed Eid, Asmaa, C.O. Olatubara, T.A. Ewemoje, Haitham Farouk, and Mohamed Talaat El-Hennawy. 2020. “Coastal Wetland Vegetation Features and Digital Change Detection Mapping based on Remotely Sensed Imagery: El-Burullus Lake, Egypt.” *International Soil and Water Conservation Research* 8: 66-79. https://doi.org/10.1016/j.iswcr.2020.01.004

Oehri, Jacqueline, Bernhard Schmid, Gabriela Schaepman-Strub, and Pascal A. Niklaus. 2017. “Biodiversity Promotes Primary Productivity and Growing Season Lengthening at the Landscape Scale.” *Proceedings of the National Academy of Sciences* 114 (38): 10160-10165. https://doi.org/10.1073/pnas.1703928114

Oliver, Tom H., Matthew S. Heard, Nick J.B. Issac, David B. Roy, Deborah Procter, Felix Eigenbrod, Rob Freckleton, Andy Hector, C. David L. Orme, Owen L. Petchey, Vânia Proença, David Raffaelli, K. Blake Suttle, Georgina M. Mace, Berta Martín-López, Ben A. Woodcock, and James M. Bullock. 2015. “Biodiversity and Resilience of Ecosystem Functions.” *Trends in Ecology & Evolution* 30 (11): 673-684. http://dx.doi.org/10.1016/j.tree.2015.08.009

Parihar, Seema Mehra, Soma Sarkar, Amitava Dutta, Shilpi Sharma, and Tanushree Dutta. 2013. “Characterizing Wetland Dynamics: A Post-Classification Change Detection Analysis of the East Kolkata Wetlands Using Open Source Satellite Data.” *Geocarto International* 28 (3): 273-287. DOI: 10.1080/10106049.2012.705337

Peterson, Seth H., Dar A. Roberts, Michael Beland, Raymond F. Kokaly, and Susan L. Ustin. 2015. “Oil Detection in the Coastal Marshes of Louisiana Using MESMA

Applied to Band Subsets of AVIRIS." *Remote Sensing of the Environment* 159: 222-231. https://10.1016.j.rse.2014.12.009

R Core Team. 2019. "R: A Language and Environment for Statistical Computing." R Foundation for Statistical Computing, Vienna, Austria. https://www.R-project.org/.

Roberts, Dar A., M. Gardner, R. Church, S. Ustin, G. Scheer, and R. O. Green. 1998. "Mapping Chaparral in the Santa Monica Mountains Using Multiple Endmember Spectral Mixture Models." *Remote Sensing of Environment* 65 (3): 267-279. https://doi.org/10.1016/S0034-4257(98)00037-6

Roberts, Dar A., P.E. Dennison, M. Gardner, Y. Hetzel, S.L. Ustin, and C. Lee. 2003. "Evaluation of the Potential of Hyperion for Fire Danger Assessment by Comparison to the Airborne Visible/Infrared Imaging Spectrometer." *IEEE Transactions on Geoscience and Remote Sensing* 41: 1297-1310.

Roberts, Dar, Kerry Halligan, Phillip Dennison, Kenneth Dudley, Ben Somers, and Ann Crabbé. 2019. "VIPER Tools" https://drive.google.com/drive/folders/0B0zkcpjAaSqFbUVacVJCSURtSzQ

Rosencranz, Jordan A., Neil K. Ganju, Richard F. Ambrose, Sandra M. Brosnahan, Patrick J. Dickhudt, Glenn R. Guntenspergen, Glen M. MacDonald, John Y. Takekawa, and Karen M. Thorne. 2016. "Balanced Sediment Fluxes in Southern California's Mediterranean-Climate Zone Salt Marshes." *Estuaries and Coasts* 39: 1035-1049. DOI 10.1007/s12237-015-0056-y

Rosso, P.H., S. L. Ustin and A. Hastings. 2005. "Mapping Marshland Vegetation of San Francisco Bay, California, Using Hyperspectral Data." *International Journal of Remote Sensing* 26 (23): 5169-5191. DOI: 10.1080/0143116050021877

Rouse, J.W., H.R. Haas, D.W. Deering, J.A. Schell, and J.C. Harlan. 1974. "Monitoring the Vernal Advancement and Retrogradation (Green Wave Effect) of Natural Vegetation." NASA/GSFC Type III Final Rep., Greenbelt, MD, 371 pp.

Silva, Germán. 2020. "Using LiDAR and Hyperspectral Data to Map Extent of Debris in Carpinteria Salt Marsh Reserve." Student paper, GEOG 214B Passive Remote Sensing, University of California Santa Barbara.

SNAP - ESA Sentinel Application Platform v8.0, http://step.esa.int

Taddeo, Sophie, Iryna Dronova, and Nicholas Depsky. 2019. "Spectral Vegetation Indices of Wetland Greenness: Responses to Vegetation Structure, Composition, and Spatial Distribution." *Remote Sensing of Environment* 234. https://doi.org/10.1016/j.rse.2019.111467

Torio, Dante D. and Gail L. Chmura. 2013. "Assessing Coastal Squeeze of Tidal Wetlands." *Journal of Coastal Research* 29 (5): 1049-1061. DOI: 10.2112/JCOASTRES-D-12-00162.1

Tuxen, Karin, L. Schile, M. Kelly, and S. Siegel. 2008. "Vegetation Colonization in a Restoring Tidal Marsh: A Remote Sensing Approach." *Restoration Ecology* 16 (2): 313-323.

Tweel, Andrew W. and R. Eugene Turner. 2012. "Landscape-Scale Analysis of Wetland Sediment Deposition from Four Tropical Cyclone Events." *PLoS ONE* 7(11): e50528. https://doi.org/10.1371/journal.pone.0050528

Uhrin, Amy V. and Jennifer Schellinger. 2011. "Marine Debris Impacts to a Tidal Fringing-Marsh in North Carolina." *Marine pollution bulletin* 62 (12): 2605-2610.

U.S Geological Survey. 2000. "Earth Explorer." *Geological Survey (U.S.)* FS 083-00

Wu, Ling, Zhaoliang Li, Xiangnan Liu, Lihong Zhu, Yibo Tang, Biyao Zhang, Boliang Xu, Meiling Liu, Yuanyuan Meng, and Boyuan Liu. 2020. "Multi-Type Forest Change Detection Using BFAST and Monthly Landsat Time Series for Monitoring Spatiotemporal Dynamics of Forests in Subtropical Wetland." *Remote Sensing* 12 (2). https://doi.org/10.3390/rs12020341

Appendix A: Code

I. Opening, reading, and classifying data

```
setwd("C:/Users/German/Desktop/Thesis/2020/11-November")#set directory to wherever the files are saved and will be saved

library(raster)
library(rgdal)
library(caret)
library(snow)
library(tidyverse)
library(wvtool)
library(randomForest)
library(calecopal)
library(ggplot2)

# open the files and save them to variables. Use raster() for single band imagery and brick() for multiband imagery
#EX:Fractions <- brick("jan_18_clipped_SMA_20201207T13H40M43S"), mARI <- raster("mARI_Jan_18.tif")
Fractions <- brick("11_12_20_clipped_SMA_20210331T13H45M44S")
NDVI <- raster("NDVI_11_12_20.tif")
ARI <- raster("mARI_11_12_20.tif")

#plot to make sure the data looks like you expect it to
#EX:plot(Fractions)
#plot(Fractions)
#plot(NDVI)
#plot(ARI)
#plot(DTM)

#DTM<-setExtent(DTM, extent(Fractions), snap = TRUE)
#DTM <- resample(DTM, Fractions, method='bilinear')

# create a layer stack with the layers you want from the data. use the $variable you see here when it was a brick variable to parse out individual layers
#Stacked_layers <- raster::stack(Fractions$BARE.SOIL_fraction,Fractions$GV_fraction,Fractions$SENESCED_fraction, Fractions$SUBTIDAL_fraction, Fractions$shade_fraction, NDVI, ARI, DTM)
Stacked_layers <- raster::stack(Fractions$BARE.SOIL_fraction,Fractions$GV_fraction,Fractions$SENESCED_fraction, Fractions$SUBTIDAL_fraction, Fractions$shade_fraction, NDVI, ARI)

#export if you wanna keep the stacked layer and use in a differnt program you can output to ENVI with filename = "example.envi", format="ENVI"
```

```
    # arcgis perfers geotiffs and won't typically open the envi files I have had
    #writeRaster(Stacked_layers, filename = "Nov_2020_stack.tif", format="GTiff",
overwrite=TRUE)

    #plot to see if all the correct lyers were attached
    #plot(Stacked_layers)

    #open stacked layers or call the layer stack variable
    img <- brick("Nov_2020_stack.tif")

    #open up the training data, i typically have 2 attribute field names of ID and
corresponding class EX: 1 Water... 2 Tree... etc.
    trainData <- shapefile("Training.shp")

    #which attribute field to call, i have found numerical variables have done better for me.
    responseCol <- "Id"

    #Extract pixel values
    #begin cluster allows you do to multicore processing and speeds up computing time.
    beginCluster()
    dfAll = data.frame(matrix(vector(), nrow = 0, ncol = length(names(img)) + 1))
    for (i in 1:length(unique(trainData[[responseCol]]))){
      category <- unique(trainData[[responseCol]])[i]
      categorymap <- trainData[trainData[[responseCol]] == category,]
      dataSet <- raster::extract(img, categorymap)
      dataSet <- sapply(dataSet, function(x){cbind(x, class =
rep(categorymap[[responseCol]], nrow(x)))})
      df <- do.call("rbind", dataSet)
      dfAll <- rbind(dfAll,df)
    }
    endCluster()

    #clean the variables of Null/NA rows/columns
    dfAll <-as.data.frame(dfAll)
    dfAll <- drop_na(dfAll)

    #model fitting and image classification. I'm sure there are more variables that can be
used in these functions
    modFit_rf <- train(as.factor(class) ~ ., method = "rf", data = dfAll, keepX= TRUE)
    beginCluster()
    preds_rf <- clusterR(img, raster::predict, args = list(model = modFit_rf))
    endCluster()
    plot(preds_rf, col= rev(cal_palette("bigsur2", n=5, type = "continuous")))

    #output final classified map
```

```
writeRaster(preds_rf, filename = "Nov_class_2020", format="GTiff", overwrite =
TRUE)
```

II. Accuracy and Data metrics

```
#importance can be inferred from Mean Decrease in Gini. Higher values mean higher
importance.
modFit_rf[["finalModel"]][["importance"]]

#class confusion/error can come from confusion matrix from the following source.
modFit_rf[["finalModel"]][["confusion"]]

#tree # / size of forest comes from
modFit_rf[["finalModel"]][["ntree"]]

#accuracy as overall and kappa value
modFit_rf[["results"]]

#Obtaining/graphing OOB error for all trees
Error_rate_11_20 <- as.data.frame(modFit_rf[["finalModel"]][["err.rate"]])

graph <- ggplot(Error_rate_11_20, aes(x= c(1:500),y=OOB))+
  geom_line()+
  labs(title="November 2020 Out of Bag (OOB) Error",x="Number of Trees",y="OOB
Error Rate")+
  theme(plot.title = element_text(size=20, face="bold",
hjust=.5),axis.text.x=element_text(size=9,face="italic"))
graph
Error_rate_11_20[500,]

#resample/K-fold
modFit_rf$resample
K_fold_11_20 <- sum(modFit_rf$resample$Accuracy)/25
K_fold_11_20
```

III. Graphing Example

```
Line graph
OOB <- read.csv("OOB_Error.csv")

colors <- c("2017/11"="#E29244", "2018/01"="#AD7E38",
"2018/11"="#58ADC5", "2020/11"="#6B6D9F")

graph <- ggplot(OOB, aes(x= c(1:500)))+
```

```
  geom_line(aes(y=OOB_11_17, color= "2017/11"))+
  geom_line(aes(y=OOB_01_18, color= "2018/01"))+
  geom_line(aes(y=OOB_11_18, color= "2018/11"))+
  geom_line(aes(y=OOB_11_20, color= "2020/11"))+
  labs(title="Out of Bag (OOB) Error",x="Number of Trees",y="OOB Error
Rate", color= "Legend")+
  scale_color_manual(values = colors)+
  theme(plot.title = element_text(size=20, face="bold",
hjust=.5),axis.text.x=element_text(size=9,face="italic"))

graph

Bar Graph
library(tidyverse)
library(ggplot2)
library(gridExtra)
library(cowplot)
library(calecopal)

gini <- read.csv("gini.csv")

gini$Date<-
factor(gini$Date,levels=unique(gini$Date)[order(gini$ID,decreasing=F)])

graph <- ggplot(gini, aes(fill=Variable, y=Gini.Value, x=Date)) +
  geom_bar(position="dodge", stat="identity")+
  labs(title="Variable Importance",y="Mean Decrease in Gini Index",x="Date")+
  scale_fill_manual(values = c("#E29244", "#F8A102", "#AD7E38",
"#58ADC5", "#5FACF8", "#4F94F7", "#5780D1", "#6B6D9F"))

graph + theme(plot.title = element_text(size=20, face="bold",
hjust=.5),axis.text.x=element_text(size=9,face="italic"))
```

Appendix B: Supplemental Figures

I. January Spectra

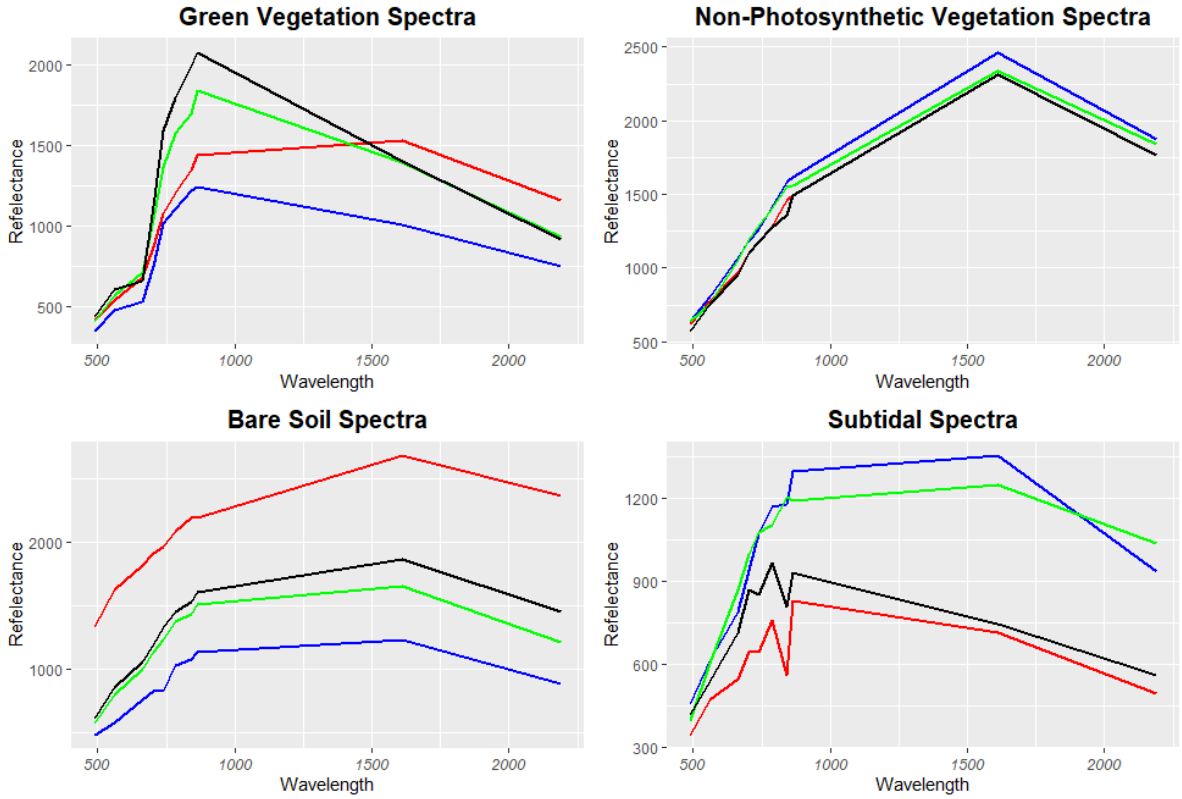

Figure 10: Spectral library for January 2018. Axes are (x) wavelength in nm and (y) reflectance values. A) non-photosynthetic vegetation spectral signatures, B) green vegetation spectral signatures, C) bare soil spectral signatures, D) subtidal spectral signatures.

II. Classification Maps

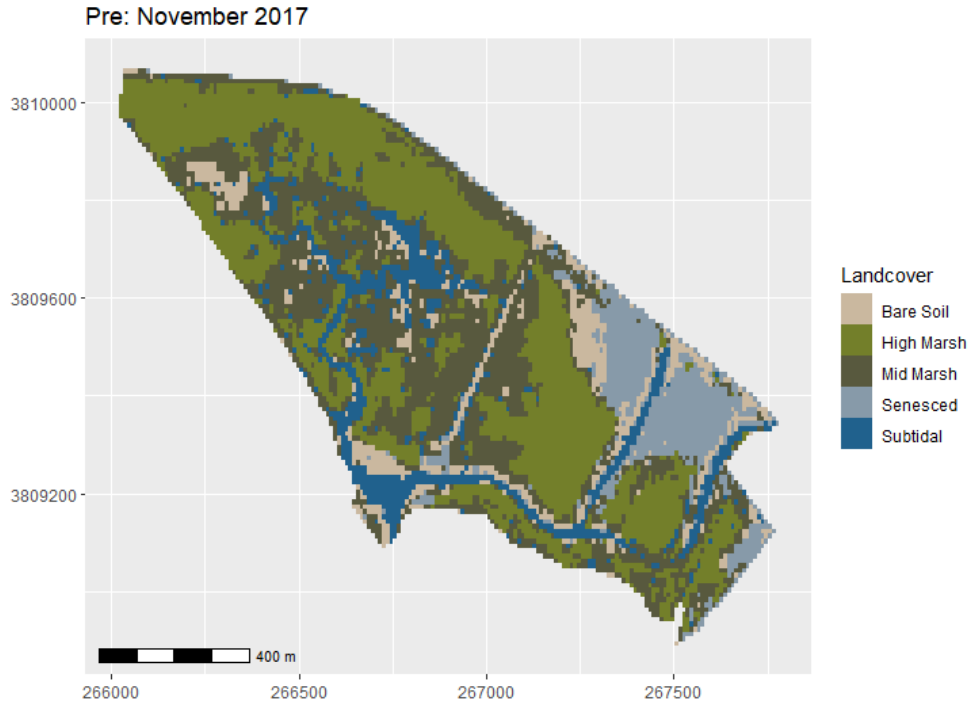

Figure 10: Random forest generated map for November 2017

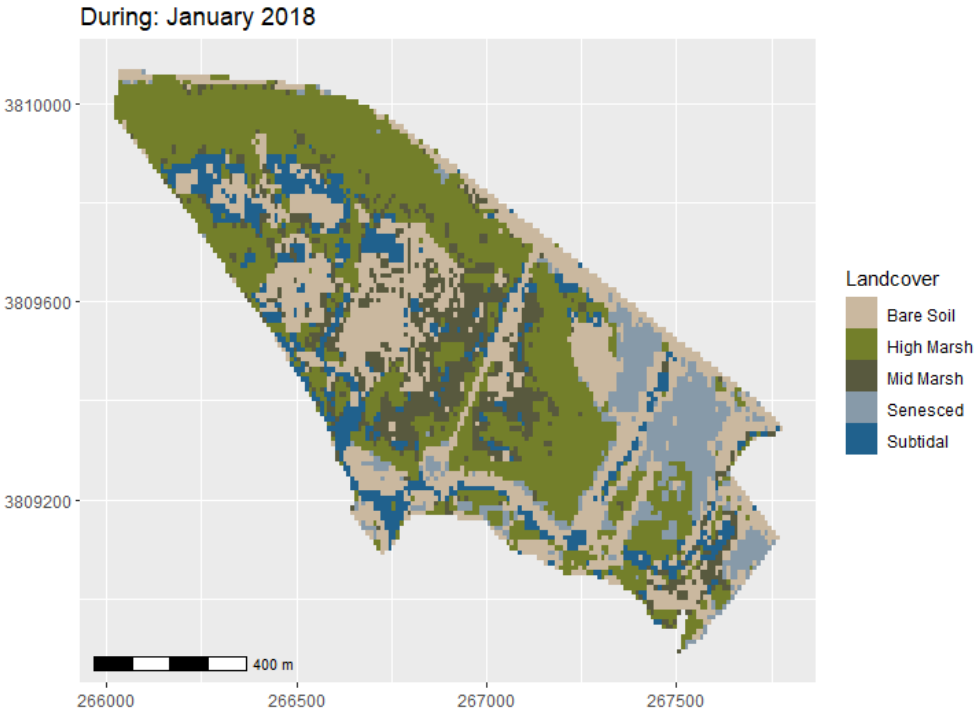

Figure 11: Random forest generated map for January 2018.

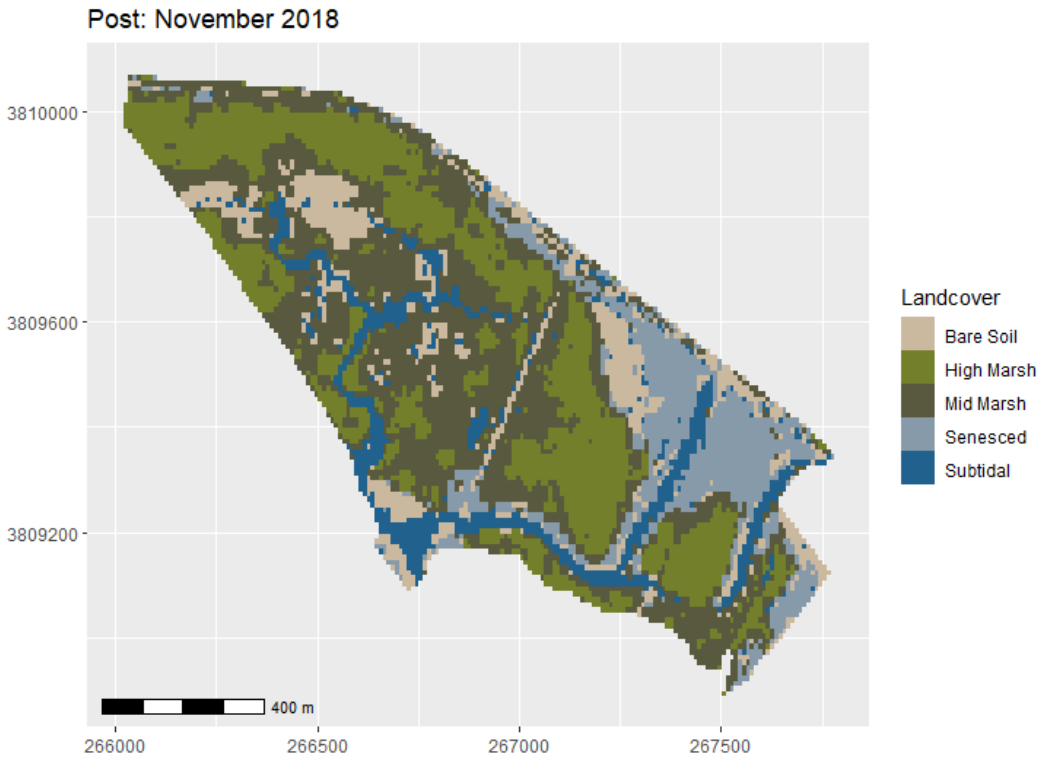

Figure 12: Random forest generated map for November 2018

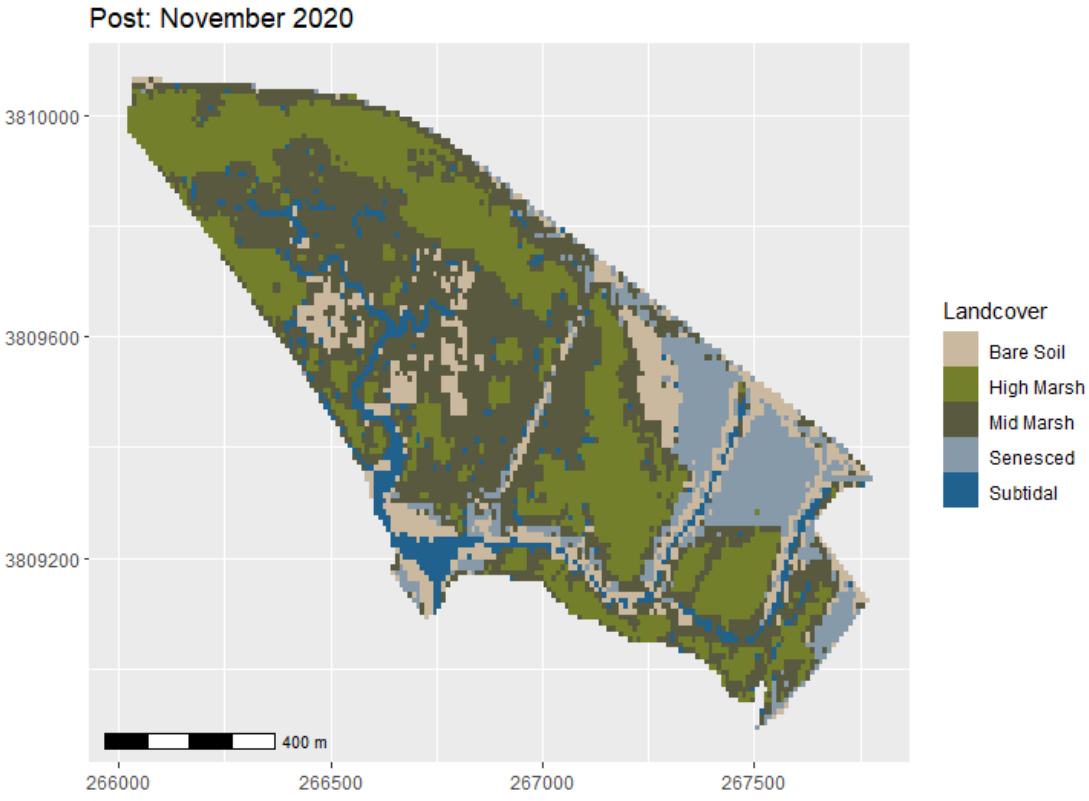

Figure 13: Random forest generated map for November 2020